IEEE Access
Multidisciplinary | Rapid Review | Open Access Journal

Received April 1, 2022, accepted April 21, 2022, date of publication April 28, 2022, date of current version May 9, 2022.

*Digital Object Identifier 10.1109/ACCESS.2022.3170889*

# Experimental Demonstration of 55-m / 2-Gbps Underwater Wireless Optical Communication Using SiPM Diversity Reception and Nonlinear Decision-Feedback Equalizer

**XIAOJIAN HONG[1,2], JI DU[2], YUAN WANG[2], RUILIN CHEN[2], JIAHAN TIAN[2], GUOWU ZHANG[2], (Graduate Student Member, IEEE), JUNWEI ZHANG[3], CHAO FEI[1,2], AND SAILING HE[1,2,4], (Fellow, IEEE)**

[1]Ningbo Research Institute, Zhejiang University, Ningbo 315100, China
[2]State Key Laboratory of Modern Optical Instrumentation, Centre for Optical and Electromagnetic Research, National Engineering Research Center for Optical Instruments, College of Optical Science and Engineering, Zhejiang University, Hangzhou 310058, China
[3]State Key Laboratory of Optoelectronic Materials and Technologies, School of Electronics and Information Technology, Sun Yat-Sen University, Guangzhou 510006, China
[4]Department of Electromagnetic Engineering, School of Electrical Engineering, Royal Institute of Technology, SE-10044 Stockholm, Sweden

Corresponding authors: Chao Fei (feichaozju@zju.edu.cn) and Sailing He (sailing@kth.se)

This work was supported in part by the National Natural Science Foundation of China (NSFC) under Grant 62001415, Grant 62101486, and Grant 62101602; in part by the National Key Research and Development Program of China under Grant 2018YFC1407503; in part by the Natural Science Foundation of Zhejiang Province under Grant LQ21F050013; in part by the Funding of Ningbo Research Institute under Grant 1141257B20200304 and Grant 1141257B20210133; in part by the Ningbo Science and Technology Project under Grant 2018B10093 and Grant 2020G012; and in part by the Fundamental Research Funds for the Central Universities.

**ABSTRACT** Underwater wireless optical communication (UWOC) is considered as an enabling technology with a mass of potential applications. The silicon photomultiplier (SiPM) exhibits a bright prospect for UWOC thanks to the traits of low-light detection capability, low-voltage operation, and superior operability. However, the performance of the SiPM-based UWOC system is severely degraded by the dead-time caused nonlinear response. In this paper, to mitigate the dead-time induced nonlinear distortion and explore the achievable capacity of the newly developed SiPM, we propose and experimentally demonstrate a 55-m / 2-Gbps UWOC system by virtue of SiPM diversity reception and nonlinear decision-feedback equalizer (NDFE). The performance of NDFE is superior to that of the conventional decision-feedback equalizer (DFE), and NDFE with a pruning factor of 5 declares similar performance as that without pruning strategy, while the number of the nonlinear equalizer can be reduced by $\sim 31.8\%$. Significant performance improvement is also obtained by the proposed scheme under different turbidity waters. The measured data rate is pushed from 1 Gbps to 2 Gbps with a receiver sensitivity as low as $-41.96$ dBm, which to the best of our knowledge is the largest data rate ever achieved using the off-the-shelf SiPM among the reported UWOC works. In accordance with the receiver sensitivity and the model of optical propagation in the water channel, the maximum attainable distance / data rate is predicted to be 147 m / 1 Gbps and 128 m / 2 Gbps with the proposed scheme. The research results are promising for long-reach and high-speed UWOC.

**INDEX TERMS** Underwater wireless optical communication (UWOC), visible laser diode (LD), silicon photomultiplier (SiPM), diversity reception, nonlinear decision-feedback equalizer (NDFE).

## I. INTRODUCTION

As the sustained growth of human activities in ocean, ranging from oceanographic study to offshore oil field exploration/monitoring, and even marine military defense, the demands for long-reach and high-speed underwater wireless communication are urgently needed [1]–[3]. Compared with the widely used underwater acoustic or radio frequency (RF) communication, which exhibits either inadequate bandwidth or heavy aquatic attenuation, underwater wireless

The associate editor coordinating the review of this manuscript and approving it for publication was Wei-Wen Hu.

**TABLE 1. Comparison of UWOC systems in recent works.**

| Year | Wavelength (nm) | Optical power | Receiver | Modulation scheme | Distance (m) | Receiver sensitivity | Data rate | Reference |
|---|---|---|---|---|---|---|---|---|
| 2017 | 520-nm LD | 19.4 mW | APD/PIN | OOK | 34.5 | -20 dBm/ >-15 dBm | 1 Gbps/ 2.7 Gbps | [6] |
| 2018 | 450-nm LD | 0.17 mW | MPPC | 4-PPM | 46 | -39.2 dBm | 5 Mbps | [24] |
| 2018 | 532-nm LD | 1 mJ single-pulse energy | PMT | 256-PPM | 120 | 3.32-bits/photon | 1.7 Mbps | [16] |
| 2019 | 520-nm LD | 7.25 mW | APD | OOK&[b]NE | 100 | -30.4 dBm/ -24 dBm | 100 Mbps/ 500 Mbps | [9] |
| 2020 | 450-nm LD | 2.4 W | MPPC | OOK | 100/50 | [a]NA | 8.39 Mbps/ 16.78Mbps | [26] |
| 2020 | 450-nm LD | 10 mW | SiPM | OOK&DFE | 40 | -43 dBm | 1 Gbps | [29] |
| 2021 | 450-nm LD | 16.18 mW | APD | DFT-S DMT | 50 | -11.2 dBm | 5 Gbps | [7] |
| 2021 | 450-nm LD | 293.1 mW | PMT | PAM4&[c]TCM | 150 | -29.8 dBm | 500 Mbps | [18] |
| 2022 | 450-nm LD | 9.88 mW | SiPM | Diversity reception &NDFE | 55 | **-49.23 dBm/ -41.96 dBm** | **1 Gbps/ 2 Gbps** | **This work** |

[a]N/A represents unavailable; [b]NE represents nonlinear equalization; [c]TCM represents Trellis coded modulation.

optical communication (UWOC) featuring low latency, large bandwidth, high flexibility, cost-effectiveness, and moderate transmission distance in water, has emerged as an enabling technology with numerous potential applications from deep sea to coastal ocean. For instance, the exchange of large volumes of gathered data (e.g., scientific data, high-resolution images, or high-quality real-time video streaming) between fixed underwater sensor nodes and remotely operated vehicles (ROVs) or autonomous underwater vehicles (AUVs) [4], [5]. Compared with the light-emitting diode (LED), the laser based UWOC system exhibits a very directive beam profile and a larger modulation bandwidth, which is more suitable for long-reach and high-speed underwater communication.

Many research groups have explored the feasibility of UWOC scenarios using the photodetectors of avalanche photodiodes (APDs) and positive-intrinsic-negative (PIN) diodes [6]–[15]. Liu *et al.* experimentally achieved 34.5-m / 2.7-Gbps underwater optical transmission using non-return-to-zero on-off keying (NRZ-OOK) modulation [6]. Du *et al.* realized 50-m / 5-Gbps underwater optical communication adopting spectrally efficient discrete Fourier transform spread discrete multi-tone (DFT-S DMT) modulation [7]. A 532-nm high-power emitting UWOC system based on 1064-nm wavelength conversion construction was experimentally demonstrated in a 100-m water tank with a data rate of 100 Mbps [8]. Using nonlinear equalization, a 100-m / 500-Mbps UWOC experiment was successfully conducted in a tap water channel [9]. However, UWOC suffers from heavy attenuation in long-distance clear water or short-distance high turbid water channels, and thus results in very weak received optical power (ROP), which poses serious challenges to the sensitivity of photodetectors.

With the merits of approaching quantum-limit sensitivity and large photosensitive area, single-photon level detectors, such as photomultiplier (PMT) and multi-pixel photon counter (MPPC), are more suitable for UWOC when ROP is extremely low or the link is not well aligned [16]–[28]. A PMT was employed as a photon-counting receiver and a 120-m / 1.7-Mbps UWOC system using 256-pulse-position modulation (PPM) was carried out in Jerlov II water [16]. The commercially available PMT-based product, namely BlueComm 200 series made by Sonardyne, was designed to support a data rate of 10 Mbps over a 150-m clear water channel [17]. Employing pulse amplitude modulation with 4 levels (PAM4), Xu *et al.* undertook the realization of a 150-m / 500-Mbps PMT-based UWOC system enabled by the combination of receiver-side partial response shaping and Trellis coded modulation [18]. Nevertheless, PMT requires careful handling as well as a high bias voltage and is susceptible to the magnetic field. Another type of highly sensitive detector MPPC, also known as arrayed single photon avalanche diode (SPAD) [22], which is comprised of a number of APDs biased above the breakdown voltage (i.e., operating in Geiger mode), has been recognized as a competitive alternative to PMT due to its high sensitivity, low operation voltage, insensitivity to the magnetic field, and mechanical robustness [23]–[29]. A 46-m / 5-Mbps MPPC-based UWOC system employing power-efficient PPM was demonstrated with a receiver sensitivity of −39.2 dBm [24]. The French Research Institute for Exploitation of the Sea (IFREMER) developed a 60-m / 3-Mbps UWOC prototype in Jerlov I water using 460-nm arrayed LED sources and arrayed MPPC receivers [25]. Zhao *et al.* adopted optical combination and arrayed MPPC to extend the transmission distance and relax the strict alignment requirement of UWOC in a 50-m standard swimming pool [26]. However, due to the limited modulation bandwidth of MPPC, the data rate of the MPPC-based UWOC system is restricted to the order of Mbps.

More recently, a newly developed commercially available MPPC, also referred to as silicon photomultiplier (SiPM),

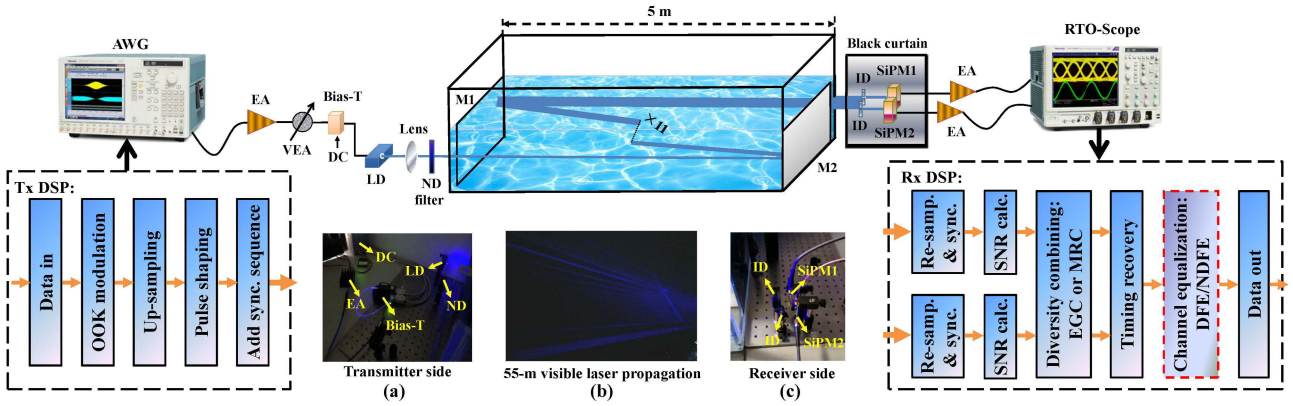


**FIGURE 1.** The schematic of the UWOC experimental setup and DSP blocks at the transmitter and the receiver side. Insets: (a) The photograph of the transmitter side; (b) an optical link of 55-m transmission in water tank; (c) The photograph of the receiver side; AWG: arbitrary waveform generator; EA: electrical amplifier; VEA: variable electrical attenuator; DC: direct current; LD: laser diode; ND filter: neutral density filter; ID: iris diaphragm; SiPM: silicon photomultiplier; RTO-Scope: real-time oscilloscope; sync.: synchronization; re-samp.: re-sampling; calc.: calculation.

was deployed in UWOC system, with which the data rate of 1 Gbps was reported over a 40-m water channel, showing excellent performance [29]. With the advantage of excellent temperature stability, high photon detection efficiency (PDE) at blue-green light, compactness, and low implementation complexity, this kind of SiPM is very suitable for deep ocean applications. However, once a photon is detected by a microcell in the SiPM, an avalanche-and-quenching process will be stimulated to bring it back to the quiescent mode. This transition occupies a finite time (several nanoseconds) and its corresponding delay is known as dead time [27], [28]. Since the microcell is unable to detect a new incoming photon during the recovery time, the number of photons detected by the SiPM is not linearly related to the intensity of the incident light. Consequently, the performance of the UWOC system will be strongly degraded by the dead-time induced nonlinear response. Nevertheless, an effective solution to alleviate such nonlinear distortion caused by the dead time effect was not involved in [29].

In this paper, to mitigate the dead-time induced nonlinear distortion and further explore the achievable capacity of the newly developed SiPM, we propose and experimentally demonstrate a 55-m / 2-Gbps UWOC system by virtue of SiPM diversity reception and nonlinear decision-feedback equalizer (NDFE). Significant performance improvement is obtained by the proposed scheme under different turbidity waters. The measured data rate is pushed from 1 Gbps to 2 Gbps with a receiver sensitivity as low as −41.96 dBm, which to the best of our knowledge is the largest data rate ever achieved using the off-the-shelf SiPM among the reported UWOC works. In accordance with the receiver sensitivity and the model of optical propagation in the water channel, the maximum attainable distance with the proposed scheme is predicted to be 147m / 1 Gbps and 128m / 2 Gbps, which is promising for long-reach and high-speed underwater transmission. Table 1 summarizes some recent works of UWOC in terms of real measured transmission distance (> 30 m), data rate, and receiver sensitivity. Note that attenuation length (AL) is a fair and critical indicator to evaluate the performance of UWOC working in different water turbidity. The lower the receiver sensitivity is, the longer the permissible transmission distance is acquired, which leads to a large AL.

The remainder of this paper is organized as follows. Section II introduces the experimental setup and principles of diversity reception and nonlinear decision-feedback equalization. The experimental results and discussions are presented in Section III. Finally, the conclusion is provided in Section IV.

## II. EXPERIMENTAL SETUP AND PRINCIPLES OF DIVERSITY RECEPTION AND NONLINEAR DECISION-FEEDBACK EQUALIZATION

Fig. 1 illustrates the schematic of the UWOC experimental setup and digital signal processing (DSP) block. As a proof-of-concept experiment, a diversity receiver consisting of two commercially available SiPM detectors (SensL J series 30035, active area of $3 \times 3$ mm$^2$) is utilized in the proposed system. At the transmitter side (Tx), an OOK modulated pseudo-random binary sequence (PRBS) is up-sampled by a factor of two, and a root-raised cosine (RRC) filter with a roll-off coefficient of 0.1 as well as a filter length of 100 are used for pulse shaping. Then the baseband shape-filtered signal is fed into an arbitrary waveform generator (AWG, Tektronix 7122C) for digital-to-analog (D / A) conversion and subsequently boosted by an electrical amplifier (EA, 10-1200MHz, 26 dB). The output RF signal with power optimized by a variable electrical attenuator (VEA) is superimposed onto the direct current (DC) via a Bias-T to drive a 450-nm single-mode pigtailed LD (Thorlabs LP450-SF15) linearly. The emitted laser beam is collimated by lens and power adjusted by a variable neutral density (ND) filter before entering a glass water tank (length: 5 m, width: 0.6 m, height: 0.3 m). A pair of parallel mirrors (M1 and M2) installed on both sides of the water tank is utilized to simulate different lengths of underwater transmission. At the receiver side (Rx), two iris diaphragms (ID) are respectively placed

in front of the detectors to adjust the ROPs. To minimize the ambient light noise, the receiver is covered by a black curtain and the measured ambient light power is about 0.1 nW. Two different operation methods, i.e., digital mode and analog mode, are provided by the manufacturer [30], in which the output signal of the former is processed by counting pulses, while in the latter, each pixel of the SiPM is directly combined together to form a summed analog output and then converted to a corresponding signal amplitude. To design a UWOC system with a large-capacity data transmission, analog mode that can support a larger modulation bandwidth is more preferred. The signal output of the SiPM is connected to a trans-impedance amplifier (TIA) with a gain of 40 dB. Finally, the detected electrical signal is digitized and stored by a real-time oscilloscope (RTO-Scope) (Tektronix, DSA72004C) for the subsequent offline signal processing. The photographs of the transmitter side, an optical link of 55-m transmission, and the receiver side are shown in Fig. 1(a)–(c), respectively. In the offline signal processing, the signal is synchronized, down-sampled, and reshaped by the same RRC filter as in the transmitter side.

Diversity combining is one of the most effective techniques for mitigating the effects brought by multipath fading and intensity fluctuation, which significantly improves the stability and reliability of the communication systems [31]–[34]. At the receiver side, the output signal after diversity combing can be characterized as:

$$Y_d = \eta_1 R_1 + \eta_2 R_2 + \cdots + \eta_N R_N = \sum_{b=1}^{N} \eta_b R_b \tag{1}$$

where $R_b$ is the received signal of the $b$-th branch, $N$is the number of diversity branches, and $\eta_b$ is the weighting coefficient of the $b$-th branch. Assuming that the noise power spectral density of the $b$-th branch is $\kappa_b$. If $\eta_b = R_b / \kappa_b$, Eq. (1) refers to as maximal ratio combing (MRC) scheme, and it becomes the optimal diversity combining, which provides the maximum signal-to-noise ratio (SNR) output. While if $\eta_1 = \eta_2 = \cdots = \eta_N$, Eq. (1) becomes the simplest combiner, but yields suboptimal performance, which refers to as equal-gain combing (EGC) scheme. In the training stage, a suitable diversity combing scheme is selected according to the measured SNR at the receiver side shown in Fig. 1. After signal diversity combining, the inter-symbol interference (ISI) mainly caused by the limited modulation bandwidth of the system can be mitigated by the decision-feedback equalizer (DFE), which consists of a transversal feed-forward equalizer (FFE) with coefficient $\alpha(k)$ and a feedback equalizer with coefficient $\gamma(i)$. The $n$-th sample of the output equalized symbols can be expressed as:

$$z(n) = \sum_{k=0}^{L-1} \alpha(k) Y_d(n-k) + \sum_{i=1}^{K} \gamma(i) \hat{d}(n-i) \tag{2}$$

where $\hat{d}(i)$ is the $i$-th sample of the decision symbols, $L$ and $K$ denote the memory length of FFE and feedback equalizer, respectively. To further mitigate the nonlinear impairment resulting from the dead-time effect of the SiPM receiver, NDFE is employed, which can be expressed as:

$$z(n) = \sum_{k_1=0}^{L_1-1} \alpha(k_1) Y_d(n-k_1) + \sum_{k_1=0}^{L_2-1} \sum_{k_2=k_1}^{L_2-1} \beta(k_1, k_2) \times Y_d(n-k_1) Y_d(n-k_2) + \sum_{i=1}^{K} \gamma(i) \hat{d}(n-i) \tag{3}$$

where $\beta(k_1, k_2)$ and $L_2$ refer to the coefficient and the memory length of the nonlinear equalizer, respectively. Since the nonlinear coefficients in the diagonal far away from the main diagonal present very small values, a straightforward strategy is to eliminate some negligible beating-terms to further reduce the complexity of NDFE. Thus, by rearranging the middle term in Eq. (3), we have:

$$\begin{aligned} z(n) = & \sum_{k_1=0}^{L_1-1} \alpha(k_1) Y_d(n-k_1) \\ & + \sum_{q=0}^{Q-1} \sum_{k=0}^{L_2-1-q} \beta(k, q+k) Y_d(n-k) Y_d(n-k-q) \\ & + \sum_{i=1}^{K} \gamma(i) \hat{d}(n-i), \quad (0 \le Q \le L_2) \end{aligned} \tag{4}$$

where $Q$ is the pruning factor. For the sake of analysis, it is preferred to describe Eq. (4) using vector notations as follows:

$$z(n) = \boldsymbol{\alpha}^T \mathbf{Y}_{n,0}^{(1)} + \sum_{q=0}^{Q-1} \boldsymbol{\beta}_q^T \left( \mathbf{Y}_{n,q}^{(2)} \odot \mathbf{Y}_{n-q,q}^{(2)} \right) + \boldsymbol{\gamma}^T \hat{\mathbf{d}}_n \tag{5}$$

where $\odot$ denotes an element-wise multiplication operation. $\boldsymbol{\alpha}$ represents the linear tap weights of the NDFE, $\boldsymbol{\beta}_q$ denotes the nonlinear tap weights of the NDFE, $\boldsymbol{\gamma}$ stands for the tap weights of the feedback equalizer, $\mathbf{Y}_{n,q}^{(k)}$ denotes the input samples for the $n$-th equalized symbol, and $\hat{\mathbf{d}}_n$ signifies the previous $K$ decision symbols. Specifically, the definitions of vectors $\boldsymbol{\alpha}$, $\boldsymbol{\beta}_q$, $\boldsymbol{\gamma}$, $\mathbf{Y}_{n,q}^{(k)}$, and $\hat{\mathbf{d}}_n$ are respectively given by:

$$\boldsymbol{\alpha} = [\alpha(0), \alpha(1), \cdots, \alpha(L_1 - 1)]^T \tag{6}$$

$$\boldsymbol{\beta}_q = [\beta(0, q), \beta(1, q+1), \cdots, \beta(L_2 - 1 - q, L_2 - 1)]^T \tag{7}$$

$$\boldsymbol{\gamma} = [\gamma(1), \gamma(2), \cdots, \gamma(K)]^T \tag{8}$$

$$\mathbf{Y}_{n,q}^{(k)} = [Y_d(n), Y_d(n-1), \cdots, Y_d(n - L_k + 1 + q)]^T, \quad k \in \{1, 2\} \tag{9}$$

$$\hat{\mathbf{d}}_n = [\hat{d}(n-1), \hat{d}(n-2), \cdots, \hat{d}(n-K)]^T \tag{10}$$

Due to the superior convergent performance, a training sequence aided recursive least-squares (RLS) algorithm [35] is firstly employed to initialize the coefficients of the equalizer, i.e.,

$$\boldsymbol{\Phi} = [\boldsymbol{\alpha}, \boldsymbol{\beta}_0, \boldsymbol{\beta}_1, \cdots, \boldsymbol{\beta}_{Q-1}, \boldsymbol{\gamma}]^T \tag{11}$$

In combination with Eq. (5) to Eq. (11), the procedure of $\hat{\boldsymbol{\Phi}}$ estimated by RLS with the training symbols $s(m)$is summarized as follows:

*Step 1:* Initialize the coefficient vector $\hat{\mathbf{\Phi}}(0) = [0, 0, \ldots, 0]^T$. Define a positive constant $\delta$ and a forgetting factor $\lambda = 0.9999$. Correlation matrix $\mathbf{\Lambda}(0) = \delta^{-1}\mathbf{I}$, where $\mathbf{I}$ is an identity matrix with the rank of $L_1 + Q(2L_2 - Q+1)/2+K$. The counter $m = 1$, and the number of training symbols is $M$.

*Step 2:* Obtain the observed vector: $\mathbf{Y}(m) = [\mathbf{Y}^{(1)}_{m,0}, \mathbf{Y}^{(2)}_{m,0} \odot \mathbf{Y}^{(2)}_{m,0}, \mathbf{Y}^{(2)}_{m,1} \odot \mathbf{Y}^{(2)}_{m-1,1}, \cdots, \mathbf{Y}^{(2)}_{m,Q-1} \odot \mathbf{Y}^{(2)}_{m-Q+1,Q-1}, \hat{\mathbf{d}}_m]$.

*Step 3:* Update the error vector according to the relation: $e(m) = s(m) - \hat{\mathbf{\Phi}}^T(m-1)\mathbf{Y}(m)$.

*Step 4:* Compute the Kalman gain vector: $\mathbf{T}(m) = \mathbf{\Lambda}(m-1)\mathbf{Y}^*(m)\left\{\lambda + \mathbf{Y}^T(m)\mathbf{\Lambda}(m-1)\mathbf{Y}^*(m)\right\}^{-1}$, and update the correlation matrix: $\mathbf{\Lambda}(m) = \lambda^{-1}\left\{\mathbf{\Lambda}(m-1) - \mathbf{T}(m)\mathbf{Y}^T(m)\mathbf{\Lambda}(m-1)\right\}$.

*Step 5:* Update the coefficient vector: $\hat{\mathbf{\Phi}}(m) = \hat{\mathbf{\Phi}}(m-1) + e(m)\mathbf{T}(m)$, increase the value of $m$, i.e., $m = m+1$, and return to Step 2 if $m < M$.

*Step 6:* After the coefficient vector $\hat{\mathbf{\Phi}}$ is fully converged, the equalizers are switched to the channel equalization stage and the received signal is equalized using $\hat{z}(n) = \hat{\mathbf{\Phi}}^T\mathbf{Y}(n)$.

Finally, the equalized symbols are recovered for bit-error-rate (BER) analysis. The structure of the NDFE using RLS is illustrated in Fig. 2. By discarding some negligible beating-terms, the complexity of the nonlinear equalizers is reduced without performance degradation, which will be presented in the following sections.

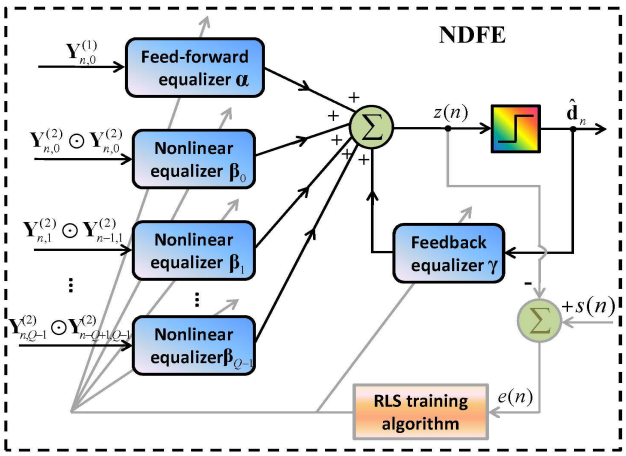


**FIGURE 2.** The schematic of the nonlinear decision-feedback equalization. The gray line shows the process of the RLS training algorithm.

## III. EXPERIMENTAL RESULTS AND DISCUSSIONS

We firstly optimize the operation conditions of the proposed SiPM-based UWOC system in a tap water channel, including the LD driving current, the control voltage of the SiPM, the memory lengths of the equalizer, and the pruning factor. Fig. 3(a) shows the output optical power and the forward voltage versus the LD driving current working at 25°C. The normalized frequency response of the back-to-back (B2B) SiPM-based UWOC system is measured by a vector network analyzer (Rohde&Schwarz ZVA40) and the result is presented in Fig. 3(b), in which the 10-dB bandwidth is approximately 500 MHz. The optimal LD driving current is ∼60 mA for different equalization schemes as shown in Fig. 3(c), corresponding to the output optical power of 9.88 mW. In Fig. 3(c) and (d), equalizers with sufficient memory lengths are utilized to obtain convergent system performance. It is observable that the performance of NDFE is superior to that of FFE and DFE. Note that the dark-count rate (DCR) is the primary source of noise in the SiPM detector, and the intrinsic characteristic indicates that the lower the DCR is, the better the SNR is obtained [30]. However, both PDE and DCR increase with the control voltage, hence there exists a tradeoff between the above two factors. Fig. 3(d) illustrates the SNR relative to the control voltage of the SiPM at a data rate of 1 Gbps. The SNR improves as the control voltage increases, implying that the contribution of PDE surpasses the negative effect of DCR. To obtain the optimal performance, the control voltage is selected as 30V. Fig. 3(e) shows the SNR versus the memory length of linear equalizer $L_1$. The SNR improves as $L_1$ increases and then reaches saturation when $L_1 = 50$. The SNR as a function of the memory length of DFE equalizer $K$ with $L_1 = 50$ is shown in Fig. 3(f). To balance the system's performance and complexity, $K$ is chosen as 16. Similarly, it is observed from Fig. 3(g) and (h) that saturated SNRs are achieved when the memory lengths of the nonlinear equalizer and the feedback equalizer of NDFE are selected as $L_2 = 11$ and $K = 13$, respectively. The measured SNR versus pruning factor $Q$ is presented in Fig. 3(i). The SNR improves with a large pruning factor and then levels off at $Q = 5$, indicating that the number of the nonlinear equalizer is reduced by ∼31.8% when we set $Q = 5$ for NDFE.

The performance of the proposed UWOC system under different turbidity waters is also experimentally investigated. Extra two different water types (''clear ocean'' and ''coastal ocean'' [36]) are obtained by adding different doses of 1% diluted Maalox$^R$ [$Al(OH)_3$ and $Mg(OH)_2$] suspension, and the corresponding attenuation coefficients ''c'' of the tap water, ''clear ocean'', and ''coastal ocean'' channel are calculated as 0.054, 0.15, and 0.41, respectively. Fig. 4 shows the BER versus ROP under different water types. The BER of single detection scheme (i.e. single-input single-output, SISO) with a data rate of 2 Gbps cannot afford 7% hard-decision forward error correction (HD-FEC) limit of BER@$3.8 \times 10^{-3}$, while significant performance enhancement is observed after utilizing the diversity combining scheme (i.e., single-input multiple-output, SIMO). Since the measured SNRs of the two branches are nearly identical, the performance of EGC is comparable to that of MRC, while EGC is more preferred due to its simplicity. As shown by the two double-headed arrows in Fig. 4, compared with the single detection, over 3-dB and 8-dB receiver sensitivity (i.e., the required ROP at the FEC limit of BER@$3.8 \times 10^{-3}$) improvement is achieved using the SIMO + DFE scheme at data rates of 1 Gbps and 2 Gbps, respectively. NDFE with a pruning factor of 5 declares similar performance as that without pruning strategy. The receiver

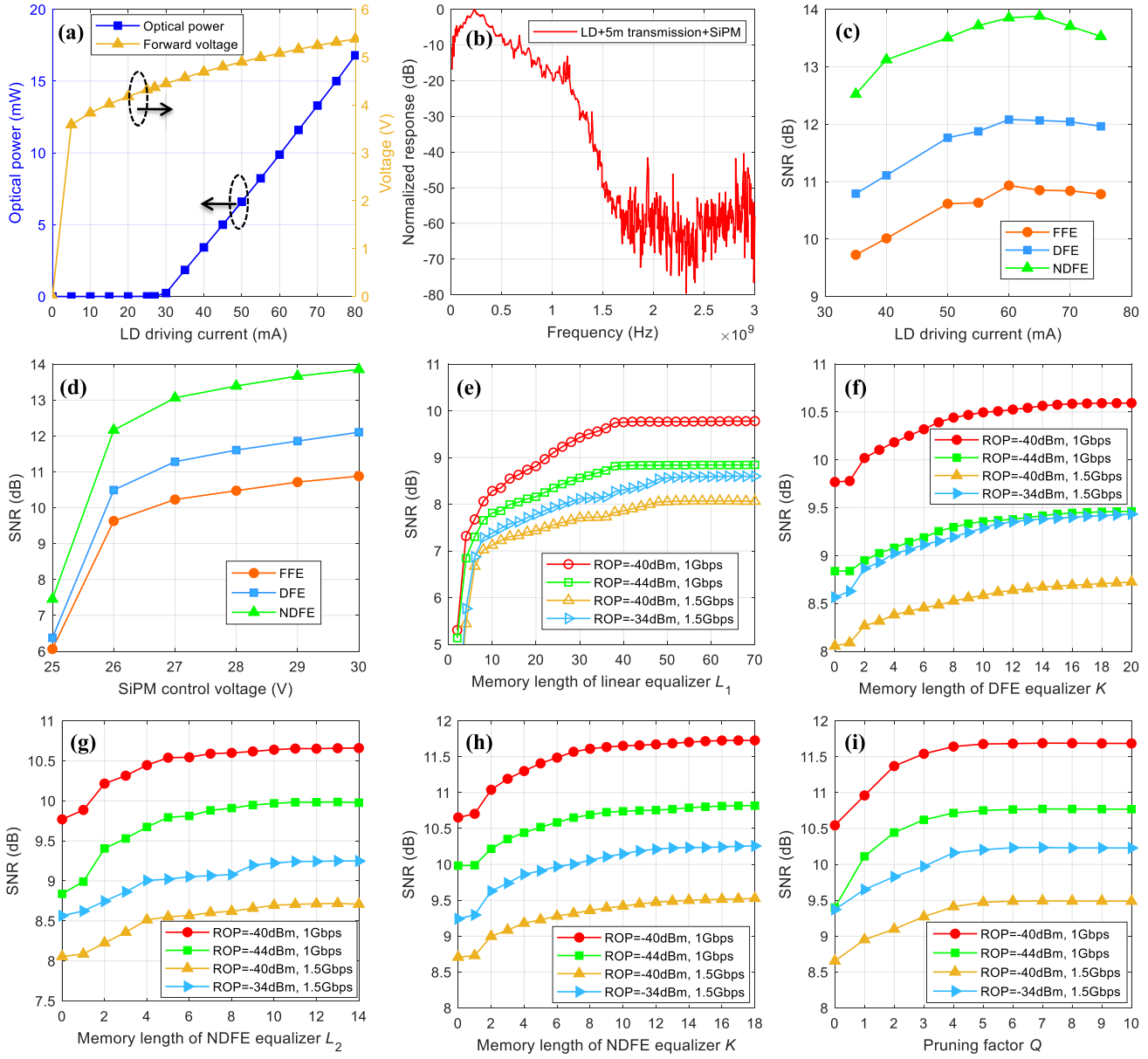


**FIGURE 3.** (a) P-I-V characteristics of the 450-nm LD working at 25°; (b) Normalized frequency response of the 5-m UWOC system; (c) SNR versus the LD driving current for different equalization schemes at a data rate of 1 Gbps; (d) SNR versus the control voltage of the SiPM at a data rate of 1 Gbps; (e) SNR versus the memory length of linear equalizer $L_1$; (f) SNR versus the memory length of DFE equalizer $K$ with $L_1 = 50$; (g) SNR versus the memory length of NDFE equalizer $L_2$ with $L_1 = 50$; (h) SNR versus the memory length of NDFE equalizer $K$ with $L_1 = 50$ and $L_2 = 11$; (i) SNR versus the pruning factor $Q$ for NDFE.

sensitivity using the proposed SIMO + NDFE ($Q = 5$) scheme is shown as −49.33 dBm / −42.0 dBm for tap water channel, −48.97 dBm / −42.75 dBm for "clear ocean" channel, and −48.98 dBm / −42.20 dBm for "coastal ocean" channel with a data rate of 1 Gbps / 2 Gbps, respectively. At the same BER, the proposed scheme requires a lower ROP, which implies that it can achieve a higher data rate or a longer transmission distance. It is noteworthy that the BER improvement behaves similar for all the transmission cases under three different water types, which exhibits the robustness of the proposed scheme.

To visualize the characteristics of the received signal, the time-domain waveform directly sampled by the RTO-Scope and the probability distributions of the received signal with different equalization schemes are presented in Fig. 5, from which we can get the following observations: 1) Significant waveform asymmetry (i.e., signal distortion) exits mainly arising from the dead time effect. 2) The probability distribution of the signal without equalization is not much like the Gaussian distribution. 3) The signal amplitude is still non-uniform after using DFE, while the probability distribution becomes uniform after using NDFE, showing the superi-

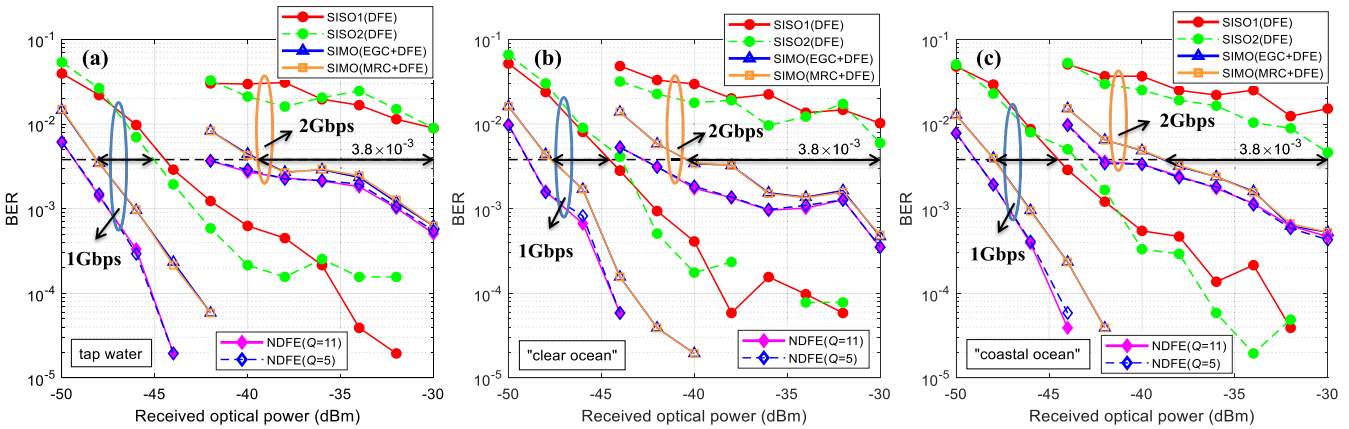


**FIGURE 4.** BER versus received optical power under different turbidity waters over a 5-m underwater channel: (a) tap water with c = 0.054; (b) "clear ocean" with c = 0.15; (c) "coastal ocean" with c = 0.41.

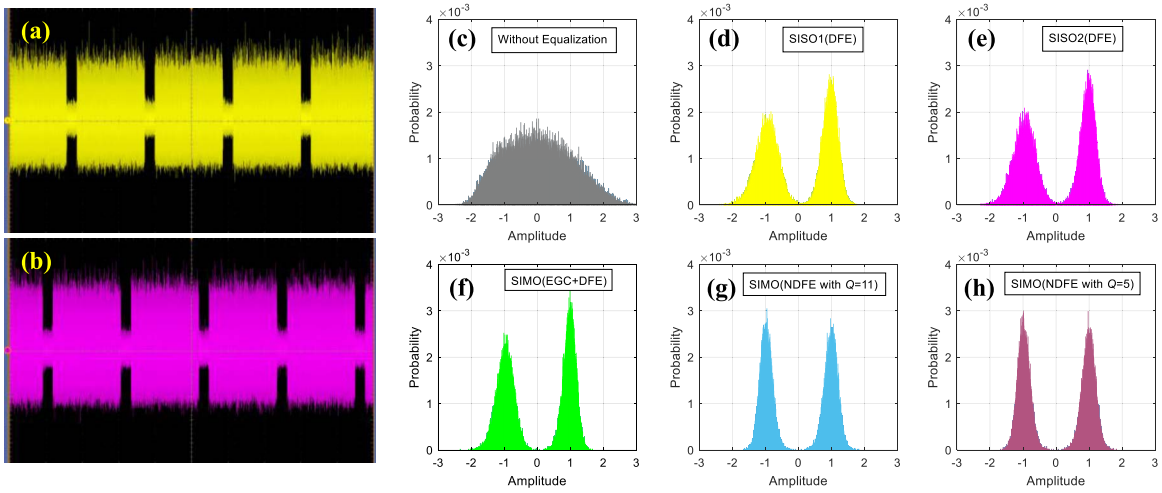


**FIGURE 5.** Time-domain waveform sampled by the RTO-Scope for (a) the SiPM1 receiver and (b) the SiPM2 receiver; The received histograms with different equalization schemes at a ROP of −40 dBm and data rate of 1 Gbps: (c) without equalization, (d) SISO1 with DFE, (e) SISO2 with DFE, (f) SIMO with EGC + DFE, (g) SIMO with EGC + NDFE ($Q = 11$), (h) SIMO with EGC + NDFE ($Q = 5$).

ority of the NDFE. 4) NDFE ($Q = 5$) with a lower complexity reveals a similar result as that without pruning strategy.

Since scattering and absorption aggravate with the increasing transmission distance, it is essential to analyze the performance of the proposed system at a longer transmission distance. The BER relative to ROP over a 55-m underwater channel is shown in Fig. 6. From the figure, the performance of the diversity reception scheme behaves similar to the results in Fig. 4, which is attributed to the light source and photodiode utilized in the proposed UWOC system. Due to a very directive beam profile, ISI induced by the water scattering is not severe in the LD-based system. Moreover, SiPM detector has a sensitivity of approaching quantum-limit. 55-m / 1-Gbps and 2-Gbps underwater transmission is successfully demonstrated employing the proposed scheme with a receiver sensitivity as low as −49.23 dBm and −41.96 dBm, respectively, which to the best of the authors' knowledge is the minimum receiver sensitivity ever achieved in the reported UWOC works with a data rate of Gbps-class. Meanwhile, compared with the results published in [29], the measured achievable data rate of the newly developed SiPM has been pushed from 1 Gbps to 2 Gbps with the proposed scheme, which is the largest ever achieved using the off-the-shelf SiPM detector among the reported UWOC works. The insets show the eye diagrams of the received signal with different equalization schemes for the UWOC system with a data rate of 1 Gbps and ROP of −46 dBm. The asymmetry of the upper / lower eyelid cannot be completely eliminated by the DFE even with the diversity reception scheme, while clearly symmetrical eye diagram is obtained using the proposed scheme with EGC + NDFE ($Q = 5$).

The receiver sensitivity improvement of the proposed scheme with SIMO + NDFE (as compared to the scheme with SISO + NDFE) versus different underwater transmission conditions is shown in Fig. 7, which intuitively presents the superiority of the diversity reception scheme. Mean-

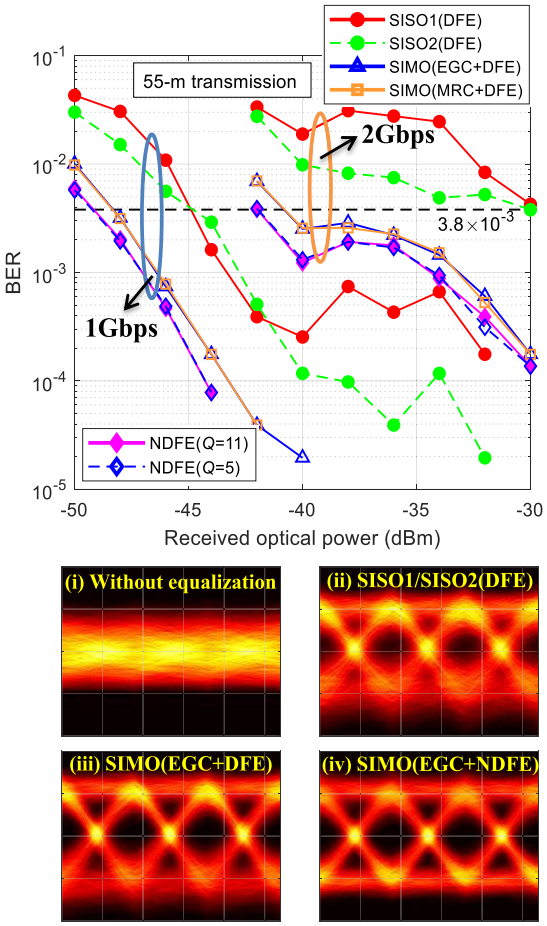


**FIGURE 6.** BER versus received optical power over a 55-m underwater channel. The insets show eye diagrams of the received signal with different equalization schemes for the UWOC system with a data rate of 1 Gbps and ROP of −46 dBm: (i) without equalization, (ii) SISO with DFE, (iii) SIMO with EGC + DFE, and (iv) SIMO with EGC + NDFE ($Q = 5$).

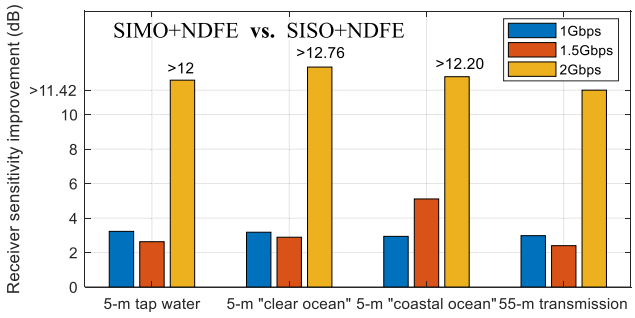


**FIGURE 7.** Measured receiver sensitivity improvement of the proposed scheme with SIMO + NDFE (as compared to the scheme with SISO + NDFE) for different underwater transmission conditions.

while, the receiver sensitivity improvement of the proposed scheme with SIMO + NDFE (as compared to the scheme with SIMO + DFE) versus different underwater transmission conditions is also shown in Fig. 8, indicating that NDFE can effectively mitigate the dead-time induced nonlinear distortion and improve the performance of the UWOC system. We can even infer that the ROP gain can be enlarged if

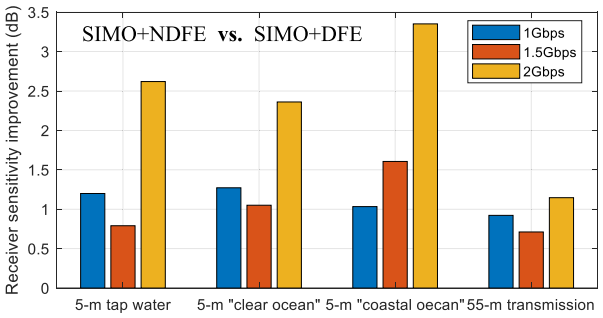


**FIGURE 8.** Measured receiver sensitivity improvement of the proposed scheme with SIMO + NDFE (as compared to the scheme with SIMO + DFE) for different underwater transmission conditions.

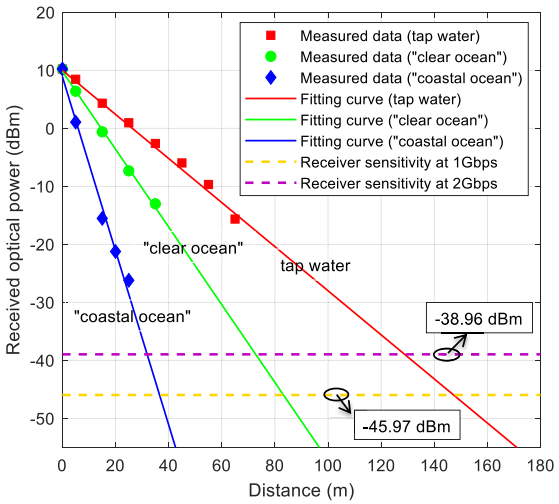


**FIGURE 9.** Received optical power versus different underwater transmission distances. The crossing point predicts the maximum achievable transmission distance at a certain data rate.

a multilevel pulse amplitude modulation signal (e.g., PAM4) is adopted in the proposed system.

The measured longest transmission distance of the proposed UWOC system is limited by the length of the water tank. Nevertheless, according to the aforementioned receiver sensitivity and the model of optical propagation (i.e., Beer-Lambert law [37]) in the water channel, it is able to predict the maximum achievable transmission distance at a certain data rate for different water types. The ROP versus different underwater transmission distances is depicted in Fig. 9. Meanwhile, the fitting curve using Beer-Lambert law is also presented. The intersection of the fitting curve and the horizontal line shows the maximum distance that can be achieved. Therefore, we can see from the figure, the transmission distances are predicted to be 147 m / 128 m for tap water channel, 83 m / 72 m for "clear ocean" channel, and 36 m / 32 m for "coastal ocean" channel with a data rate of 1 Gbps / 2 Gbps, respectively. Meanwhile, the achievable maximum AL is predicted to be 7.94, 12.45, and 14.76 for the above three water types at a data rate of 1 Gbps. It can be even envisioned that a longer UWOC transmission distance can be acquired if the data rate is relaxed or a higher power delivery of LD is available.

## IV. CONCLUSION

We have proposed and experimentally demonstrated an SiPM diversity reception based UWOC system using diversity combing and NDFE. NDFE can effectively ease the dead-time induced nonlinear distortion as compared to the conventional DFE scheme, and significant performance improvement is demonstrated with the proposed scheme under three different water types. Furthermore, 55-m / 1-Gbps and 2-Gbps underwater transmission is also successfully demonstrated using the proposed scheme with a receiver sensitivity as low as −49.23 dBm and −41.96 dBm, respectively, which is competitive both in data rate and receiver sensitivity among the reported UWOC works. According to the measured receiver sensitivity and the model of optical propagation in the water channel, the longest transmission distance is predicted to be 147 m / 1 Gbps and 128 m / 2 Gbps. Meanwhile, the achievable maximum AL is predicted to be 7.94, 12.45, and 14.76 for tap water, ''clear ocean'', and ''coastal ocean'' channel respectively at a data rate of 1 Gbps. The research results forecast promising application of the SiPM diversity reception based UWOC system and meet the requirements of long-reach and high-speed underwater transmission. In future work, we will verify the performance of the proposed scheme in outdoor field test.

## REFERENCES

[1] H. Kaushal and G. Kaddoum, ''Underwater optical wireless communication,'' *IEEE Access*, vol. 4, pp. 1518–1547, 2016.

[2] B. Shihada, O. Amin, C. Bainbridge, S. Jardak, O. Alkhazragi, T. K. Ng, B. Ooi, M. Berumen, and M. S. Alouini, ''Aqua-Fi: Delivering internet underwater using wireless optical networks,'' *IEEE Commun. Mag.*, vol. 58, no. 5, pp. 84–89, May 2020.

[3] Z. Zeng, S. Fu, H. Zhang, Y. Dong, and J. Cheng, ''A survey of underwater optical wireless communications,'' *IEEE Commun. Surveys Tuts.*, vol. 19, no. 1, pp. 204–238, 1st Quart., 2017.

[4] N. Saeed, A. Celik, T. Y. Al-Naffouri, and M.-S. Alouini, ''Underwater optical wireless communications, networking, and localization: A survey,'' *Ad Hoc Netw.*, vol. 94, Nov. 2019, Art. no. 101935.

[5] J. Xu, ''Underwater wireless optical communication: Why, what, and how?'' *Chin. Opt. Lett.*, vol. 17, no. 10, 2019, Art. no. 100007.

[6] X. Liu, S. Yi, X. Zhou, Z. Fang, Z. Qiu, L. Hu, C. Cong, L. Zheng, R. Liu, and P. Tian, ''34.5 m underwater optical wireless communication with 2.70 Gbps data rate based on a green laser diode with NRZ-OOK modulation,'' *Opt. Exp.*, vol. 25, no. 22, pp. 27937–27947, Oct. 2017.

[7] J. Du, Y. Wang, C. Fei, R. Chen, G. Zhang, X. Hong, and S. He, ''Experimental demonstration of 50-m/5-Gbps underwater optical wireless communication with low-complexity chaotic encryption,'' *Opt. Exp.*, vol. 29, no. 2, pp. 783–796, 2021.

[8] Y. Yang, L. Fan, F. He, Y. Song, Z. Duan, Y. Zhu, and B. Li, ''Long-distance underwater optical wireless communication with PPLN wavelength conversion,'' *Proc. SPIE*, vol. 11717, Dec. 2020, Art. no. 117172J.

[9] J. Wang, C. Lu, S. Li, and Z. Xu, ''100 m/500 Mbps underwater optical wireless communication using an NRZ-OOK modulated 520 nm laser diode,'' *Opt. Exp.*, vol. 27, no. 9, pp. 12171–12181, Apr. 2019.

[10] X. Sun, M. Kong, O. Alkhazragi, K. Telegenov, M. Ouhssain, M. Sait, Y. Guo, B. H. Jones, J. S. Shamma, T. K. Ng, and B. S. Ooi, ''Field demonstrations of wide-beam optical communications through water–air interface,'' *IEEE Access*, vol. 8, pp. 160480–160489, 2020.

[11] W.-S. Tsai, H.-H. Lu, H.-W. Wu, C.-W. Su, and Y.-C. Huang, ''A 30 Gb/s PAM4 underwater wireless laser transmission system with optical beam reducer/expander,'' *Sci. Rep.*, vol. 9, no. 1, pp. 1–8, Dec. 2019.

[12] N. Chi and M. Shi, ''Advanced modulation formats for underwater visible light communications,'' *Chin. Opt. Lett.*, vol. 16, no. 12, 2018, Art. no. 120603.

[13] Y.-F. Huang, C.-T. Tsai, Y.-C. Chi, D.-H. Huang, and G.-R. Lin, ''Filtered multicarrier OFDM encoding on blue laser diode for 14.8-Gbps seawater transmission,'' *J. Lightw. Technol.*, vol. 36, no. 9, pp. 1739–1745, May 1, 2018.

[14] C. Fei, X. Hong, G. Zhang, J. Du, Y. Wang, and S. He, ''Improving the performance of long reach UOWC with multiband DFT-spread DMT,'' *IEEE Photon. Technol. Lett.*, vol. 31, no. 16, pp. 1315–1318, Aug. 15, 2019.

[15] Y. Shao, R. Deng, J. He, K. Wu, and L.-K. Chen, ''Real-time 2.2-Gb/s water-air OFDM-OWC system with low-complexity transmitter-side DSP,'' *J. Lightw. Technol.*, vol. 38, no. 20, pp. 5668–5675, Oct. 15, 2020.

[16] S. Hu, L. Mi, T. Zhou, and W. Chen, ''35.88 attenuation lengths and 3.32 bits/photon underwater optical wireless communication based on photon-counting receiver with 256-PPM,'' *Opt. Exp.*, vol. 26, no. 17, pp. 21685–21699, 2018.

[17] [Online]. Available: https://www.sonardyne.com/product/bluecomm-200-wireless-underwater-video/

[18] X. Chen, X. Yang, Z. Tong, Y. Dai, X. Li, M. Zhao, Z. Zhang, J. Zhao, and J. Xu, ''150 m/500 Mbps underwater wireless optical communication enabled by sensitive detection and the combination of receiver-side partial response shaping and TCM technology,'' *J. Lightw. Technol.*, vol. 39, no. 14, pp. 4614–4621, Jul. 15, 2021.

[19] C. Fei, Y. Wang, J. Du, R. Chen, N. Lv, G. Zhang, J. Tian, X. Hong, and S. He, ''100-m/3-Gbps underwater wireless optical transmission using a wideband photomultiplier tube (PMT),'' *Opt. Exp.*, vol. 30, no. 2, pp. 2326–2337, 2022.

[20] C. Li, Z. Liu, D. Chen, X. Deng, F. Yan, S. Li, and Z. Hu, ''Experimental demonstration of high-sensitivity underwater optical wireless communication based on photocounting receiver,'' *Photonics*, vol. 8, no. 467, p. 467, 2021.

[21] T. Liu, H. Zhang, Y. Zhang, and J. Song, ''Experimental demonstration of LED based underwater wireless optical communication,'' in *Proc. 4th Int. Conf. Inf. Sci. Control Eng. (ICISCE)*, Jul. 2017, pp. 1501–1504.

[22] C. Wang, H. Y. Yu, and Y. J. Zhu, ''A long distance underwater visible light communication system with single photon avalanche diode,'' *IEEE Photon. J.*, vol. 8, no. 5, pp. 1–11, Oct. 2016.

[23] L. Zhang, H. Chun, Z. Ahmed, G. Faulkner, D. O'Brien, and S. Collins, ''The future prospects for SiPM-based receivers for visible light communications,'' *J. Lightw. Technol.*, vol. 37, no. 17, pp. 4367–4374, Sep. 1, 2019.

[24] J. Shen, J. Wang, X. Chen, C. Zhang, M. Kong, Z. Tong, and J. Xu, ''Towards power-efficient long-reach underwater wireless optical communication using a multi-pixel photon counter,'' *Opt. Exp.*, vol. 26, no. 18, pp. 23565–23571, Aug. 2018.

[25] P. Leon, F. Roland, L. Brignone, J. Opderbecke, J. Greer, M. Bigand, M. A. Khalighi, T. Hamza, and S. Bourennane, ''A new underwater optical modem based on highly sensitive silicon photomultipliers,'' in *Proc. OCEANS-Aberdeen*, Jun. 2017, pp. 1–6.

[26] M. Zhao, X. Li, X. Chen, Z. Tong, W. Lyu, Z. Zhang, and J. Xu, ''Long-reach underwater wireless optical communication with relaxed link alignment enabled by optical combination and arrayed sensitive receivers,'' *Opt. Exp.*, vol. 28, no. 23, pp. 34450–34460, 2020.

[27] J. Li, D. Ye, K. Fu, L. Wang, J. Piao, and Y. Wang, ''Single-photon detection for MIMO underwater wireless optical communication enabled by arrayed LEDs and SiPMs,'' *Opt. Exp.*, vol. 29, no. 16, pp. 25922–25944, 2021.

[28] M. A. Khalighi, T. Hamza, S. Bourennane, P. Léon, and J. Opderbecke, ''Underwater wireless optical communications using silicon photomultipliers,'' *IEEE Photon. J.*, vol. 9, no. 4, Aug. 2017, Art. no. 7905310.

[29] L. Zhang, X. Tang, C. Sun, Z. Chen, Z. Li, H. Wang, R. Jiang, W. Shi, and A. Zhang, ''Over 10 attenuation length gigabits per second underwater wireless optical communication using a silicon photomultiplier (SiPM) based receiver,'' *Opt. Exp.*, vol. 28, no. 17, pp. 24968–24980, 2020.

[30] [Online]. Available: https://www.onsemi.com/products/sensors/photodetectors-sipm-spad/silicon-photomultipliers-sipm/j-series-sipm

[31] M. S. Alouini, S. W. Kim, and A. Goldsmith, ''RAKE reception with maximal-ratio and equal-gain combining for DS-CDMA systems in Nakagami fading,'' in *Proc. 6th Int. Conf. Universal Pers. Commun.*, vol. 2, Oct. 1997, pp. 708–712.

[32] M. A. Khalighi and M. Uysal, ''Survey on free space optical communication: A communication theory perspective,'' *IEEE Commun. Surveys Tuts.*, vol. 16, no. 4, pp. 2231–2258, 4th Quart., 2014.

[33] F. Wang, Y. Liu, F. Jiang, and N. Chi, ''High speed underwater visible light communication system based on LED employing maximum ratio combination with multi-PIN reception,'' *Opt. Commun.*, vol. 425, pp. 106–112, Oct. 2018.

[34] W. Liu, Z. Xu, and L. Yang, "SIMO detection schemes for underwater optical wireless communication under turbulence," *Photon. Res.*, vol. 3, no. 3, pp. 48–53, Oct. 2015.
[35] J. G. Proakis and M. Salehi, *Digital Communications*, 5th ed. New York, NY, USA: McGraw-Hill, 2007, ch. 10.
[36] F. Hanson and S. Radic, "High bandwidth underwater optical communication," *Appl. Opt.*, vol. 47, no. 2, pp. 277–283, 2008.
[37] C. Gabriel, M.-A. Khalighi, S. Bourennane, P. Leon, and V. Rigaud, "Monte-Carlo-based channel characterization for underwater optical communication systems," *J. Opt. Commun. Netw.*, vol. 5, no. 1, pp. 1–12, 2013.

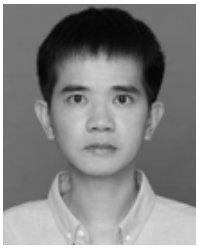

**XIAOJIAN HONG** received the B.S. and M.S. degrees from South China Normal University, Guangzhou, China, in 2013 and 2016, respectively, and the Ph.D. degree in optical communication technology from Zhejiang University, Hangzhou, China, in 2020. He is currently an Assistant Professor with the Ningbo Research Institute and the College of Optical Science and Engineering, Zhejiang University. His research interests include digital signal processing, underwater wireless optical communication, and visible light communication.

**JI DU** received the B.S. degree in engineering ocean technology from the Dalian University of Technology, Liaoning, China, in 2018. He is currently pursuing the Ph.D. degree with the College of Optical Science and Engineering, Zhejiang University, Hangzhou, China. His research interests include underwater wireless optical communication and visible light communication.

**YUAN WANG** received the B.S. degree in communication engineering from Central South University, Changsha, China, in 2019. She is currently pursuing the Ph.D. degree with the College of Optical Science and Engineering, Zhejiang University, Hangzhou, China. Her research interests include underwater wireless optical communication and visible light communication.

**RUILIN CHEN** received the B.S. degree in optoelectronic information science and engineering from Harbin Engineering University, Harbin, China, in 2020. He is currently pursuing the M.S. degree with the College of Optical Science and Engineering, Zhejiang University, Hangzhou, China. His research interests include underwater wireless optical communication and visible light communication.

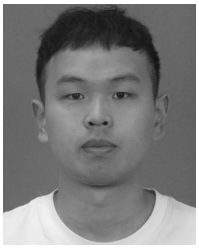

**JIAHAN TIAN** received the B.S. degree in optical and electronic information science and engineering from the Huazhong University of Science and Technology, Wuhan, China, in 2020. He is currently pursuing the M.S. degree with the College of Optical Science and Engineering, Zhejiang University, Hangzhou, China. His research interests include optical fiber communication and indoor optical wireless communication.

**GUOWU ZHANG** (Graduate Student Member, IEEE) received the B.S. degree in optical information science and engineering from the Huazhong University of Science and Technology, Wuhan, China, in 2015, and the M.S. degree in optical engineering from Zhejiang University, Hangzhou, China, in 2018. He is currently pursuing the Ph.D. degree in electric engineering with the Department of Electronic and Computer Engineering, McGill University, Montreal, QC, Canada. His research interests include optical communication, computational nanophotonic device design, and optical switch.

**JUNWEI ZHANG** received the B.S. and M.S. degrees in information engineering and optical engineering from South China Normal University, Guangzhou, China, in 2014 and 2017, respectively, and the Ph.D. degree in optical engineering from Sun Yat-Sen University, Guangzhou, in 2020. He is currently a Postdoctoral Fellow with Sun Yat-Sen University. His research interests include optical communication systems and digital signal processing.

**CHAO FEI** received the B.S. degree in information engineering form the Changshu Institute of Technology, Suzhou, China, in 2012, the M.S. degree in optical engineering from the South China Normal University, Guangzhou, China, in 2015, and the Ph.D. degree in optical communication technology from Zhejiang University, Hangzhou, China, in 2019. He is currently an Assistant Professor with the Ningbo Research Institute and the College of Optical Science and Engineering, Zhejiang University. His research interests include visible light communication and underwater wireless optical communication.

**SAILING HE** (Fellow, IEEE) received the Lic. and Ph.D. degrees in electromagnetic theory from the KTH Royal Institute of Technology, Stockholm, Sweden, in 1991 and 1992, respectively.

He was an Assistant Professor, an Associate Professor, and a Full Professor of electromagnetic theory at the KTH Royal Institute of Technology. He is also a Professor with Zhejiang University (ZJU), China, and the Director of the KTH-ZJU Joint Research Centre of Photonics (JORCEP). He has first authored one monograph (Oxford University Press) and authored or coauthored over 700 articles in refereed international journals. His current research interests include sub-wavelength photonics, sensing technologies, optical communication, and applied electromagnetics. He is a fellow of the Optical Society of America (OSA), the International Society for Optical Engineering (SPIE), and The Electromagnetics Academy.